Activity-based protein profiling in drug-discovery

Esbroeck, A.C.M. van

6

Summary & future prospects

The aim of this thesis was to explore activity-based protein profiling (ABPP) as a tool in drug discovery and cell biology.

Chapter 1 discussed the different phases of the drug discovery process, such as target discovery and hit identification. ABPP is introduced as a versatile chemical tool, which may aid in addressing these challenges. ABPP employs active site-directed probes to assess the functional state of an entire enzyme class (e.g. serine hydrolases and kinases) in complex protein samples. Fluorescently labeled activity-based probes (ABPs) allow rapid analysis of the functional state of the enzymes by in-gel fluorescence scanning, whereas probes with affinity tags enable target enrichment and identification by mass spectrometry (MS)[1,2]. The ABPP methodology can be used in a comparative setup to map the activity landscape of different biological samples (e.g. healthy versus diseased) (Figure 1A). Alternatively, a competitive setup with inhibitors can be used for target engagement studies or selectivity profiling (Figure 1B).

The serine hydrolases play a central role in the research performed in this thesis. They represent a large protein family (~ 1% of the mammalian proteome) and are involved in a broad spectrum of physiological processes, including signaling and metabolism[2]. In the described work, a special focus was set on the serine hydrolases of the endocannabinoid system (ECS), which were also introduced in **Chapter 1**.

The ECS regulates a broad spectrum of physiological and pathological processes, including memory, pain, anxiety, appetite, metabolism and inflammation. The versatile role of the ECS in physiology makes the ECS interesting for therapeutic exploitation[3,4]. The ECS is comprised of the cannabinoid receptor type 1 and 2 (CB1R, CB2R), their endogenous ligands, the endocannabinoids 2-arachidonoylglycerol (2-AG) and anandamide (AEA), and their metabolic enzymes[5]. Diacylglycerol lipase α and β (DAGLα, DAGLβ) are the two main 2-AG biosynthetic enzymes[6]. Monoacylglycerol lipase (MGLL) and α,β-hydrolase domain containing protein 6 and 12 (ABHD6, ABHD12) can terminate 2-AG signaling by its hydrolysis to arachidonic acid (AA) and glycerol[7–10]. There are multiple AEA biosynthetic pathways, but hydrolysis of *N*-acylphosphatidyl-ethanolamines (NAPEs) to *N*-acylethanolamines (NAEs, including AEA), by NAPE phospholipase D (NAPE-PLD) is considered to be the canonical pathway[11]. Fatty acid amide hydrolase (FAAH) hydrolyzes the NAEs to ethanolamines and free fatty acids[12,13]. With the exception of NAPE-PLD, all endocannabinoid metabolic enzymes are part of the serine hydrolase family.

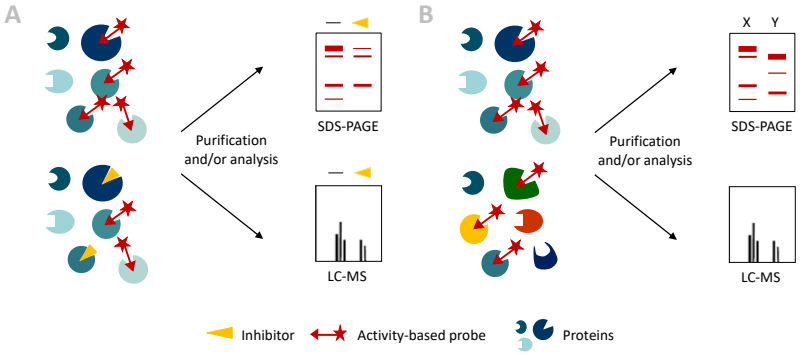

Figure 1 | Schematic representation of competitive (A) and comparative (B) ABPP.

Chapter 2 demonstrated comparative ABPP as a tool for rapid mapping of the serine hydrolase activity profile in ischemic cardiac tissue. The endocannabinoids and their receptors have emerged as important modulators of the cardiovascular system, especially under diseased conditions[14–16]. The role of endocannabinoid metabolizing enzymes, however, has been investigated less extensively. Cardiac tissues from patients with terminal-stage heart failure (due to previous ischemic pathology) and non-failing control hearts were used to determine the endocannabinoid levels and the activity of the endocannabinoid hydrolases. mRNA expression of *DAGL*β, *MGLL*, *ABHD6* and *NAPEPLD* was decreased in the ischemic tissues. Two subgroups were identified within the ischemic group by lipidomics and ABPP analysis; the first similar to control hearts and the second with reduced levels of the endocannabinoid 2-AG and drastically increased levels of AEA, NAEs and free fatty acids. The aberrations in the lipid profile were accompanied by decreased activity of 13 hydrolases, including the 2-AG hydrolytic enzyme MGLL. The distinct profiles of the two ischemic subgroups indicate the existence

of differential biological states and may be related to more severe cardiac damage in the second subgroup, based on the significant reduction in cardiac output and the increase in systemic vascular resistance within this patient group.

In a similar setup as described in **Chapter 2**, comparative ABPP has contributed to the discovery of novel therapeutic targets or biomarkers for a variety of clinical indications. For example, in cancer research, the strength of the technique was demonstrated by the identification of enhanced MGLL activity in aggressive human cancer cells and primary tumors. Overexpression of MGLL in non-aggressive cancer cells increased their pathogenicity and the effects could be reversed with a MGLL inhibitor[17]. Similarly, elevated levels of KIAA1363 activity were detected in aggressive cancer cells. Inhibition of this hydrolase disrupted lipid metabolism in cancerous cells, thereby impairing cell migration and tumor growth *in vivo*[18]. Upon further investigation, MGLL and KIAA1363 may serve as biomarkers for tumor malignancy and as therapeutic targets for the treatment of certain aggressive tumors.

In **Chapter 3**, the ABPP methodology was extended to an *in vivo* model system. Recently, the zebrafish (*Danio rerio*) has emerged as a model system for embryonic development.[19,20] Furthermore, zebrafish larvae are increasingly used as a pre-clinical vertebrate model in drug discovery[21,22] and toxicological screening[23–25]. Thus far, most biochemical studies were limited to protein[26,27] and gene expression[28,29] profiles, whereas the protein activity component was often not taken into account. This limitation was addressed in **Chapter 3**, which described the development of an ABPP method for broad-spectrum profiling of serine hydrolase and kinase activity in zebrafish larvae. ABPP coupled to MS-analysis enabled the identification and mapping of 45 hydrolases (including ECS-related MGLL, ABHD6a, ABHD12 and FAAH2a) and 51 kinases throughout early zebrafish development (0-5 days post fertilization). The number of detected hydrolases and kinases increased during development and could be correlated to specific developmental processes. **Chapter 3** also showcased how zebrafish larvae can be used as pre-clinical animal model for *in vivo* target engagement and selectivity screening. FAAH inhibitor PF04457845 was used in a competitive ABPP setup and was found to be a highly selective compound. Inhibitor uptake and downstream effects on the lipid profile were confirmed using MS-based methods.

Phenotypic screening in intact animals, rather than in a single cell type, takes the complexity of the complete organism into account. For example, dorsomorphin, an inhibitor of the bone morphogenetic protein (BMP) (ALK8 in zebrafish, ALK2 in humans), was discovered in a phenotypic screen, because it triggered dorsalization in early zebrafish embryogenesis. Its target was identified based on phenotypic similarity to larvae carrying a genetic *Alk8* mutation[21,30]. The large collection of zebrafish phenotypes associated with specific genetic mutations has been an effective tool for target identification in the past[21]. Nevertheless, without a phenotypic match target identification remains challenging, especially when the phenotype is the result of

simultaneous modulation of multiple targets. In such cases, competitive ABPP can serve as a valuable tool for target identification and selectivity profiling, complementary to existing methods. In addition, *in vivo* treatment of the larvae can provide a rapid readout for basic toxicological studies during hit/lead identification and optimization, while monitoring inhibitor selectivity by competitive ABPP. Likewise, comparative ABPP may aid in target discovery by identifying altered enzyme activities in zebrafish disease models.

In **Chapter 4**, competitive ABPP was used to investigate the interaction landscape of FAAH inhibitor BIA 10-2474. A recent phase I clinical trial with this inhibitor resulted in the death of one volunteer and hospitalization of four others with mild-to-severe neurological symptoms[31–34]. Considering the clinical safety profile of other FAAH inhibitors, it was postulated that off-target activities of BIA 10-2474 may have played a role. In a competitive ABPP assay with human brain lysates, BIA 10-2474 was a poorly potent, but apparently selective FAAH inhibitor with ABHD6 as the only off-target. However, BIA 10-2474's inhibitory potency towards recombinant FAAH, FAAH2 (a human FAAH orthologue) and ABHD6 improved drastically in a cellular system. In this light, the *in situ* interaction landscape of BIA 10-2474 was investigated in human cortical neurons and three additional off-targets were identified; patatin-like phospholipase domain containing protein 6 (PNPLA6), carboxyl esterase 2 (CES2) and phospholipase 2 group XV (PLA2G15). Importantly these lipases, except for FAAH and FAAH2, were not targeted by PF04457845, a highly selective and clinically safe FAAH inhibitor[35,36]. Prolonged BIA 10-2474, but not PF04457845, exposure produced substantial alterations in the lipid network of primary neurons, in accordance with the role of the BIA 10-2474 targets in cellular lipid metabolism. BIA 10-2474 thus acts a promiscuous lipase inhibitor, with the potential to cause metabolic dysregulation in the nervous system, which in turn may have contributed to the observed clinical neurotoxicity. The relative causality of the identified BIA 10-2474 off-targets, however, could not be established in this study, because clinical samples of the patients were not available. Integration of chemical proteomics in the drug discovery workflow as a tool to assess on-target engagement and off-target activity may guide therapeutic development and will hopefully contribute to the safety of clinical trials.

Remarkably, prolonged *in situ* BIA 10-2474 treatment (48 h) of HEK293-T cells recombinantly expressing ABHD6 or FAAH resulted in accumulation of inhibited ABHD6 protein, but not of inhibited FAAH protein (Figure 2A). This effect was mimicked using ABHD6 inhibitor KT195[37] (Figure 2A) and similar increases in ABHD6 levels were obtained in a second human cell line (U2-OS) as well as in the murine cell line Neuro-2a (Figure 2B). No other BIA 10-2474 targets accumulated upon inhibition (Figure 2C). These data suggest that the increase in ABHD6 protein levels is not due to general interference with protein metabolism or biosynthesis, but rather suggests that ABHD6 proteostasis is modulated specifically upon its inhibition. Some enzyme inhibitors are known to act as chemical chaperones increasing cellular protein levels by reducing

proteolysis or by enhancing protein biosynthesis and folding[38], and BIA 10-2474 and KT195 may function as such. Of note, no suitable antibodies were available to study the effect of ABHD6 inhibition on endogenous protein levels. Alternatively, BIA 10-2474 analogs AJ167, AJ179, and AJ198 (described in Chapter 4) containing a bio-orthogonal ligation handle, were used to enable target visualization using two-step ABPP. However, these analogs did not inhibit ABHD6 substantially (Figure 2D).

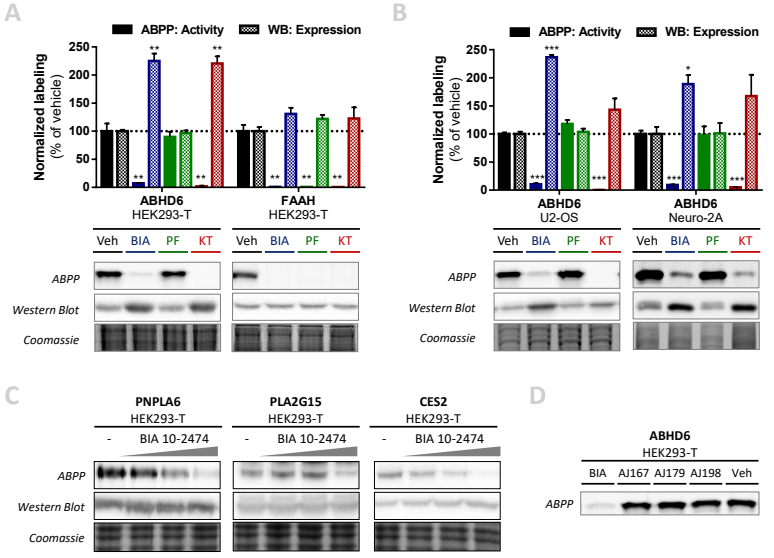

Figure 2 | ABHD6, but no other BIA 10-2474 targets, accumulates upon BIA 10-2474 inhibition. (**A**-**B**) HEK293-T (**A**), U2-OS, and Neuro-2a (**B**) cells were transiently transfected with FLAG-tagged ABHD6 (**A**, **B**) or FAAH (**A**). Cells were treated *in situ* with vehicle, BIA 10-2474 (10 µM), PF04457845 (1 µM), or KT 195 (10 µM) for 48 h. Protein activity and expression was analyzed by gel-based ABPP with FP-TAMRA (500 nM) (**A**) or MB064 (250 nM) (20 min, rt) (**B**) and western blot against the FLAG-tag. Coomassie staining served as a protein loading control. Labeling was quantified and normalized for protein loading and is expressed as % of vehicle (mean ± SEM (n=3), *t*-test with Holm-Sidak multiple comparison correction: * $p < 0.05$, ** $p < 0.01$, *** $p < 0.001$). (**C**) HEK293-T cells were transiently transfected with FLAG-tagged PNPLA6, PLA2G15 or CES2 and were treated *in situ* with vehicle or BIA 10-2474 (1, 10, 100 µM) for 48 h. Protein activity and expression was analyzed by gel-based ABPP with FP-TAMRA (500 nM, 20 min, rt) and western blot against the FLAG-tag. Coomassie staining served as a protein loading control. (**D**) HEK293-T cells were transiently transfected with ABHD6 and treated *in situ* with vehicle, BIA 10-2474, AJ167, AJ179, or AJ198 (10 µM, 48 h). ABHD6 activity is visualized by gel-based ABPP with probe MB064 (250 nM, 20 min, rt) (n=2).

The accumulation of inhibited ABHD6 is especially relevant considering the scaffolding function of ABHD6, which is independent of its catalytic function. ABHD6 acts as a potent negative regulator of cell surface trafficking of GluR1-subunit of the α-amino-3-hydroxy-5-methyl-4-isoxazolepropionic acid receptors (AMPARs), one of the major postsynaptic ionotropic glutamate receptors mediating excitatory synaptic neurotransmission in the central nervous system. Provided that endogenous ABHD6 also accumulates upon inhibition, BIA 10-2474 may cause aberrations in AMPAR-mediated glutamatergic signaling as a result of ABHD6 accumulation, which in turn may contribute to BIA 10-2474's clinical neurotoxicity. Electrophysiological studies will be valuable in

assessing the effects of BIA 10-2474 and ABHD6 inhibition on glutamatergic signaling and thus on excitotoxicity.

In **Chapter 5** ABPP is employed to identify the enzymes involved in neuronal differentiation. Retinoic acid (RA)-stimulation of Neuro-2a cells was previously shown to induce neurite outgrowth and to increase cellular 2-AG levels[39]. The contribution of endogenously expressed DAGLα and DAGLβ was investigated using pharmacological, genetic, and chemical proteomic methods. DAGL inhibitor DH376 completely abolished cellular 2-AG levels and delayed RA-induced neuronal differentiation. Surprisingly, CRISPR/Cas9-mediated knockdown (KD) of the 2-AG biosynthetic DAGLα and DAGLβ in Neuro-2a cells did not affect cellular 2-AG levels, suggesting the presence of other enzymes capable of 2-AG biosynthesis. A bio-orthogonal ligation handle in DH376 enabled target identification by chemical proteomics. DAGLβ and ABHD6 were identified as the only DH376-targets in Neuro-2a cells. ABHD6 has been reported as a promiscuous lipase that uses 2-AG, as well as various lysophosphatidyl species[40] and bis(monoacylglycero)phosphate[41] as substrates. Biochemical, genetic and lipidomic studies revealed that ABHD6 possesses diacylglycerol (DAG) lipase activity in conjunction with its previously reported role as a monoacylglycerol (MAG) lipase. During RA-induced differentiation an elevation of ABHD6 activity was observed along with a reduction in DAGLβ activity, suggesting a physiological role of ABHD6 in 2-AG signaling.

The exact physiological role of ABHD6 in 2-AG metabolism, however, is difficult to assess due to its dual MAG and DAG lipase activities. It is likely that the reactions are driven by the relative substrate and product concentrations. This could be further studied using radiolabeled substrates. Triple DAGL and ABHD6 KO mice may also provide information on the physiological role of ABHD6 in 2-AG signaling. In a dual DAGLα and DAGLβ knockout mouse model, brain 2-AG levels were not completely abolished[42] and it is tempting to speculate that ABHD6 may account for the remainder of the 2-AG content.

In the study by Jung and colleagues, RA-induced differentiation was mediated by CB1R[39]. Notably, in **Chapter 5** both 2-AG and AEA levels increased during RA-induced differentiation, suggesting that either endocannabinoid may be responsible for the CB1R-mediated effects in differentiating Neuro-2a cells. Remarkably, also other NAE levels increased during differentiation, ranging from a 2- to a 15-fold increase (Figure 3). These pronounced alterations propose a role of the NAEs in neuronal differentiation. The NAE *N*-docosahexaenoylethanolamine (DHEA, synaptamide) has already been described as a potent neurogenic metabolite. A biotinylated DHEA analog enabled affinity purification of the DHEA interaction partners and resulted in the identification of G-protein coupled receptor 110 (GPR110) as the synaptamide receptor mediating the neurogenic effects of DHEA[43]. Similar approaches could enable identification of the interaction partners of other NAEs and may thereby contribute to understanding their role in neuronal differentiation.

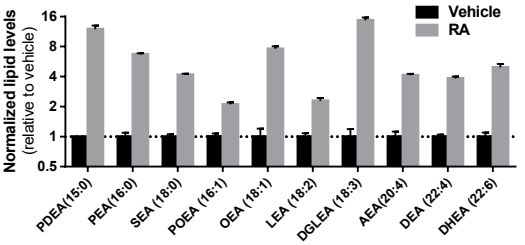

Figure 3 | NAE levels increase during RA-induced differentiation of Neuro-2a. Neuro-2a cells were stimulated by *in situ* treatment with retinoic acid (RA, 50 µM, 2 % serum, 72 h). Lipids were extracted and analyzed by LC-MS/MS. Lipid abundance was normalized to the number of cells. Data is expressed as a fraction of vehicle (mean ± SEM (n=5)). Vehicle and RA-treatment are statistically significant with $p < 0.001$ for all NAE's (*t*-test with Holm-Sidak multiple comparison correction).

To investigate the role of AEA and the NAE's in differentiation, NAPE-PLD and FAAH KD populations were generated (Figure 4). Over 90% KD efficiency was reached based on western blot analysis (Figure 4A, C). Upon NAPE-PLD KD, most NAEs were strongly reduced, including AEA (Figure 4B). KD of FAAH resulted in elevated levels of a few NAE species, but not of AEA (Figure 4D), suggesting the existence of other AEA metabolic pathways in these cells. Automation of the neurite outgrowth analysis, e.g. with applications like NeuriteTracer[44], is required to properly assess the differentiation process over time. Fluorescence imaging instead of phase contrast imaging, which was used in **Chapter 5,** would significantly aid these types of studies. Comparison of Neuro-2a WT and KD populations during differentiation, as well as the effects of spiking endocannabinoids and NAEs to the differentiation medium may help establish the role of these lipids in RA-induced differentiation in Neuro-2a.

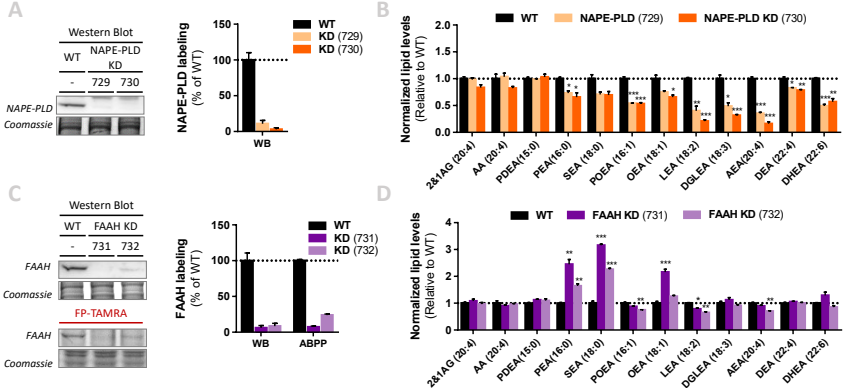

Figure 4 | NAE levels are altered in Neuro-2a NAPE-PLD and FAAH KD populations. (**A**-**D**) Neuro-2a KD populations of NAPE-PLD (**A**-**B**) and FAAH (**C**-**D**) were generated by three sequential transfections with Cas9 and two separate guides for each target (NAPE-PLD: 729, 730; FAAH: 731, 732). (**A**, **C**) Western blot showed a high KD efficiency of NAPE-PLD and FAAH using antibodies against each target. FAAH activity was strongly decreased in FAAH KD populations, based on gel-based ABPP using FP-TAMRA (500 nM, 20 min, rt). Labeling was quantified and is expressed as % of vehicle (mean ± SEM, n=3). (**B**, **D**) Lipids were extracted from WT and KD cells and analyzed by LC-MS/MS. Lipid abundance was normalized for the amount of protein. Data is expressed as a fraction of vehicle (mean ± SEM (n=4), *t*-test with Holm-Sidak multiple comparison correction: * $p < 0.05$, ** $p < 0.01$, *** $p < 0.001$).

Opportunities and challenges in ABPP

The continuous development of the ABPP methodology contributes to its maturation and further extend on its already versatile character. Novel broad-spectrum probes targeting other protein classes will increase the biological reach of the technique, whereas highly specific probes enable alternative experimental approaches, e.g. imaging enzyme activity in living cells, assessing subcellular localization of active protein using correlative light and electron microscopy (CLEM)[45], or visualizing activity *in vivo* using ABPs containing a positron emission tomography (PET) radiotracer[46]. The development of new analytical platforms and analysis methods can improve the experimental throughput and provide new experimental approaches to biological questions. For example, the recently developed label-free quantification method for chemical proteomics[47] enables comparison of multiple sample types within one experiment. This analysis method circumvents the previously required sample pairing, which could lead to distortions due to divergence between biological replicates. Technical advances in MS-analysis will contribute to further exploitation of ABPP as a tool in cellular biology, for example by facilitating the characterization of post-translational modifications (PTMs)[48] in intact proteins (top-down proteomics)[49].

Further integration of competitive ABPP in the drug discovery process is a promising perspective for this method. In target-based drug discovery, activity assays with purified enzyme often serve as the primary screening method[50]. By taking the proteins out of their biological context, external factors such as protein-protein interactions cannot be accounted for. This may result in limited *in vitro* to *in situ*/*in vivo* translatability. For now, high-throughput screening (HTS)-compatible ABPP assays, such as fluorescence polarization[51] and EnPlex[52] still require the use of purified protein. However, these techniques do have major advantages as they do not require prior knowledge on the enzyme's substrate and (with limited modifications) the same assay can be used for other targets of the same ABP. After hit identification, gel- and MS-based ABPP can guide the lead optimization and preclinical phases, by enabling rapid assessment of potency and selectivity within the native proteome and in biologically relevant systems. Patient-derived inducible pluripotent stem cells (iPSCs) may provide particularly promising disease models and may proof valuable in competitive ABPP approaches for phenotype- and target-based drug discovery.

Even though the competitive ABPP method provides a lot of information on the inhibitor interaction profile, it is still limited to the enzymes that react with the probe. In the case of covalent inhibitors, a ligation handle can aid identification of covalent targets (e.g. DH376 in Chapter 5). However, incorporation of a ligation handle may change the inhibitor reactivity and selectivity, as was observed for the BIA 10-2474 alkyne derivatives in Figure 2. Non-covalent targets may be identified using a photoactivatable group, which interacts covalently with the associated proteins after UV-irradiation. In a similar fashion, non-enzymatic proteins, e.g. receptors, can be targeted using these so called photoaffinity probes[53].

Conclusion

Taken together, this thesis described several ABPP strategies and applications in drug discovery and cell biology (Figure 5). In a comparative setup, ABPP enabled rapid assessment of clinical samples to identify molecular role players in disease, which may lead to the discovery of novel therapeutic targets or biomarkers. Competitive ABPP, on the other hand, provides information on the drug interaction landscape. It enabled target engagement studies and inhibitor selectivity profiling, as demonstrated with BIA 10-2474, an inhibitor that caused severe neurological symptoms in a phase I clinical trial. Integration of competitive ABPP in preclinical testing will provide better insight in drug selectivity and drug safety. In zebrafish larvae the comparative ABPP methodology served as a tool to map the kinase and serine hydrolase landscape throughout embryonic development, thereby providing new activity-based insights in embryonic development. In addition, competitive ABPP in these larvae enabled *in vivo* target engagement and selectivity profiling. Lastly, a combined approach of ABPP, CRISPR/Cas9-mediated genetic modification, biochemistry and lipidomics resulted in the identification of ABHD6 as a 2-AG biosynthetic diacylglycerol lipase in retinoic acid-induced differentiation of Neuro-2a.

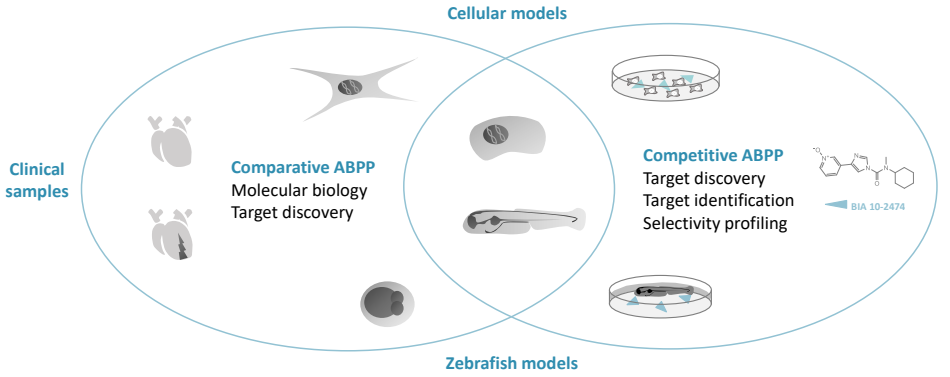

Figure 5 | Visual summary of ABPP strategies and their applications described in this thesis.

To conclude, activity-based protein profiling is a versatile and powerful chemical tool and its integration in cell biology and drug discovery research is anticipated to bring forward new insights in both research fields.

Experimental procedures

Materials, probes, and inhibitors

Fluorophosphonate-TAMRA (FP-TAMRA) was purchased from Thermo Fisher. MB064, BIA 10-2474, AJ167, AJ179, AJ198 were synthesized as previously described[54,55]. All synthesized compounds were at least 95% pure and were analyzed by LC/MS, NMR, and HRMS. Primers were ordered from Sigma Aldrich or Integrated DNA Technologies. Other chemicals and reagents were purchased from Sigma Aldrich, unless indicated otherwise.

Cloning

Full-length human cDNA of ABHD6, FAAH, PNPLA6, PLA2G15, CES2 (Source Bioscience) was cloned into mammalian expression vector pcDNA3.1, containing genes for ampicillin and neomycin resistance. The inserts were cloned in frame with a C-terminal FLAG-tag and site-directed mutagenesis was used to remove restriction sites by silent point mutations. pcDNA3.1 containing the gene for eGFP was used as a transfection control. Plasmids were isolated from transformed XL-10 Z-competent cells (Maxi Prep kit: Qiagen) and sequenced at the Leiden Genome Technology Center. Sequences were analyzed and verified (CLC Main Workbench).

Cell Culture

General

HEK293-T (human embryonic kidney), U2-OS (human osteosarcoma) and Neuro-2a (murine neuroblastoma) cells were cultured at 37 °C under 7% CO_2 in DMEM containing phenol red, stable glutamine, newborn bovine serum (10%, v/v; Thermo Fisher), and penicillin and streptomycin (200 µg/mL each; Duchefa). Medium was refreshed every 2-3 days and cells were passaged twice a week at ~ 90% confluence by resuspension in fresh medium (HEK293-T, Neuro-2a) or trypsinization (U2-OS). Cell lines were purchased from ATCC and were regularly tested for mycoplasma contamination. Cultures were discarded after 2-3 months of use.

Transient transfections

One day prior to transfection, cells were seeded at $0.3*10^6$ cells/well in a 12-wells plate. Prior to transfection, culture medium was aspirated and a minimal amount of complete medium was added. A mixture (HEK293-T, U2-OS: 3:1 (m/m); Neuro-2a: 5:1 (m/m)) of polyethyleneimine (PEI) and plasmid DNA (0.625 µg/well) was prepared in serum-free culture medium and incubated (15 min, rt). Transfection was performed by dropwise addition of the PEI/DNA mixture to the cells. Transfection with pcDNA3.1 encoding GFP or empty pcDNA3.1 vector was used to generate control samples. 24 h Post-transfection culture medium was refreshed. Transfection efficiency was checked by fluorescence microscopy on eGFP-transfected samples (EVOS FL2 Auto, GFP-channel).

In situ treatments

Cells from transient transfections were used at 24h post-transfection. Culture medium was aspirated and after a careful PBS wash treatment medium containing vehicle (0.1% DMSO) or inhibitor (1-100 µM as indicated in figure legends) was added. After incubation for 48 h at 37 °C and 7% CO_2, treatment medium was aspirated and cells were carefully washed with PBS. Subsequently cells were harvested by resuspension or scraping in PBS and were spun down (1000 *g*, 3-5 min, rt). Cell pellets were flash frozen in liquid nitrogen and stored at -80 °C until further use.

CRISPR/Cas9 knockdowns

Guide design & constructs

Two sgRNA's, in early exons, with high efficiency and specificity as predicted by CHOPCHOP v2 online web tool[56] (http://chopchop.cbu.uib.no) were selected. Guides were cloned into the BbsI restriction site of plasmid px330-U6-Chimeric_BB-CBh-hSpCas9 (gift from Feng Zhang, Addgene plasmid #42230) as previously described[57,58]. Constructs and primers are annotated in Table 1.

Knockdown population generation

Neuro-2a cells were transfected sequentially to yield populations with a high knockdown efficiency. The full experimental procedure is provided in **Chapter 5**. After three transfection rounds, the cells were cultured according to standard protocol. Knockdown efficiency was determined by T7E assay, gel-based ABPP and western blot. Ampoules of knockdown populations were prepared (complete DMEM, 10% DMSO) and stored at -150 °C. Cells were discarded after 3 months of culture.

Table 1 | sgRNA targets, sgRNA oligos (top, bottom) and T7E1 primers (forward, reverse).

sgRNA Target	Construct	Primer Sequences	
***Nape-pld* – Exon 2**	729	Top: Bottom:	CACCGATAGCTTGGCGCTGGAGAC AAACGTCTCCAGCGCCAAGCTATC
– Exon 3	730	Top: Bottom:	CACCAGTTCGCTTATTGTACACGG AAACCCGTGTACAATAAGCGAACT
Faah **– Exon 1**	731	Top: Bottom:	CACCGCGCTGCACCGCCTTGTCCA AAACTGGACAAGGCGGTGCAGCGC
– Exon 2	732	Top: Bottom:	CACCGAATCCAGGTCAGGATTCTG AAACCAGAATCCTGACCTGGATTC

Whole lysate preparation

Cell pellets were thawed on ice, resuspended in cold lysis buffer (20 mM HEPES pH 7.2, 2 mM DTT, 250 mM sucrose, 1 mM $MgCl_2$, 2.5 U/mL benzonase) and incubated on ice (15 min). Protein concentrations were determined by a Quick Start™ Bradford Protein Assay (Bio-Rad). After dilution to 2 mg/mL in sucrose lysis buffer or storage buffer (20 mM HEPES pH 7.2, 2 mM DTT), samples were used or flash frozen in liquid nitrogen and stored at -80 °C until further use. DTT was left out of all buffers for samples intended for click-chemistry.

Activity-based protein profiling

Whole lysate (2 mg/mL) was incubated with activity-based probes MB064 (250 nM, 20 min, rt) or FP-TAMRA (500 nM, 20 min, rt). The reaction was quenched with Laemmli buffer (30 min, rt) and 20 µg protein was resolved by SDS-PAGE (10% acrylamide gel) along with protein marker PageRuler™ Plus (Thermo Fisher). In-gel fluorescence was detected in the Cy3- and Cy5-channel on a ChemiDoc™ MP imaging system (Bio-Rad) and gels were stained with coomassie after scanning. Fluorescence was quantified and normalized to coomassie staining using ImageLab™ software (Bio-Rad) and data was processed in Excel (Microsoft) and GraphPad Prism 7 (GraphPad).

Western blot

Cell lysates were denatured with Laemmli buffer (30 min, rt) and 20 µg lysate was resolved on a 10% acrylamide SDS-PAGE gel along with PageRuler™ Plus Protein Marker (Thermo Scientific). Proteins were transferred to 0.2 µm polyvinylidene difluoride membranes by Trans-Blot Turbo™ Transfer system (Bio-Rad). Membranes were washed with TBS (50 mM Tris, 150 mM NaCl) and blocked with 5% milk in TBS-T (50 mM Tris, 150 mM NaCl, 0.05% Tween 20) (1 h, rt). Membranes

were subsequently incubated with primary antibody mouse-anti-FLAG (F3156, Sigma Aldrich; 1:5000 in 5% milk in TBS-T, 45 min at rt or O/N at 4 °C), rabbit-anti-NAPE-PLD (ab95397, Abcam; 1:200 in TBS-T, O/N, 4 °C), or mouse-anti-FAAH (CST2942, Cell Signaling Technologies; 1:1000 in 5% milk in TBS-T, O/N, 4 °C). After incubation membranes were washed with TBS-T and incubated with secondary goat-anti-mouse-HRP or goat-anti-rabbit-HRP (sc-2005, sc-2004, Santa Cruz Biotechnologies; 1:5000 in 5% milk TBS-T, 45 min, rt) and washed with TBS-T and TBS. Chemilumescence (developed with ECL) was detected on the ChemiDoc™ MP (Bio-Rad) in the chemiluminessence channel, and colorimetric channel for the protein marker. Signal was normalized to coomassie staining using ImageLab™ software (Bio-Rad) and data was processed in Excel (Microsoft) and GraphPad Prism 7 (GraphPad).

Lipidomics

Sample preparation: Neuro-2a retinoic acid stimulation

Neuro-2a cells were seeded at $0.75*10^6$ cells/dish in a 10 cm dish. One day after seeding, medium was aspirated and retinoic acid stimulation was initiated by adding DMEM containing 2% serum and retinoic acid (50 µM) or vehicle (0.1% DMSO). After 72 h neurite outgrowth was investigated using phase contrast microscopy (Olympus). Cells were carefully washed with PBS and harvested by resuspension in PBS (for retinoic acid stimulated cells, 5 dishes were combined to yield sufficient cells). Cells were pelleted (200 *g*, 10 min, rt) and resuspended in 1 mL PBS. Cell count and viability were checked by Trypan blue staining and automated cell counting (TC20™ Cell Counter, Bio-Rad) and $2*10^6$ cells were pelleted (1000 *g,* 3 min, rt). Pellets were flash frozen in liquid nitrogen and stored at -80 °C until lipid extraction.

Sample preparation: Neuro-2a knockdown populations

Neuro-2a cells (WT or KD) were seeded at $2*10^6$ cells/dish in a 10 cm dish. Cells were harvested when confluence was reached. Culture medium was aspirated and cells were resuspended in DMEM. Cell count and viability were checked by Trypan blue staining and automated cell counting (TC20™ Cell Counter, Bio-Rad) and $2*10^6$ cells were pelleted (1000 *g,* 3 min, rt) (n=3 pellets). Pellets were washed twice with PBS (5 min, 1000 *g*), flash frozen in liquid nitrogen and stored at -80 °C until lipid extraction.

Lipid extraction & LC-MS/MS Analysis

Lipid extraction was performed as previously described[55] with minor adaptations. The full experimental procedure is provided in **Chapter 5**.

Statistical methods

Experiments were performed in an appropriate number of replicates, as indicated in figure legends. A *t*-test was used to determine statistical significance, with Holm-Sidak multi-comparison correction using GraphPad Prism 7 (GraphPad). Samples were compared to vehicle or wildtype controls and statistical significance is indicated as * $p < 0.05$, ** $p < 0.01$, *** $p < 0.001$.

References

1. Niphakis, M. J. & Cravatt, B. F. Enzyme Inhibitor Discovery by Activity-Based Protein Profiling. *Annu. Rev. Biochem.* **83,** 341–377 (2014).
2. Liu, Y., Patricelli, M. P. & Cravatt, B. F. Activity-based protein profiling: The serine hydrolases. *Proc. Natl. Acad. Sci.* **96,** 14694–14699 (1999).
3. Mechoulam, R. & Parker, L. A. The Endocannabinoid System and the Brain. *Annu. Rev. Psychol.* **64,** 21–47 (2012).
4. Di Marzo, V., Bifulco, M. & De Petrocellis, L. The endocannabinoid system and its therapeutic exploitation. *Nature Reviews Drug Discovery* **3,** 771–784 (2004).
5. Di Marzo, V. Endocannabinoid signaling in the brain: biosynthetic mechanisms in the limelight. *Nat. Neurosci.* **14,** 9–15 (2011).
6. Bisogno, T. *et al.* Cloning of the first sn1-DAG lipases points to the spatial and temporal regulation of endocannabinoid signaling in the brain. *J. Cell Biol.* **163,** 463–468 (2003).
7. Dinh, T. P., Freund, T. F. & Piomelli, D. A role for monoglyceride lipase in 2-arachidonoylglycerol inactivation. in *Chemistry and Physics of Lipids* **121,** 149–158 (2002).
8. Marrs, W. R. *et al.* The serine hydrolase ABHD6 controls the accumulation and efficacy of 2-AG at cannabinoid receptors. *Nat. Neurosci.* **13,** 951–7 (2010).
9. Blankman, J. L., Simon, G. M. & Cravatt, B. F. A comprehensive profile of brain enzymes that hydrolyze the endocannabinoid 2-arachidonoylglycerol. *Chem. Biol.* **14,** 1347–1356 (2007).
10. Savinainen, J. R., Saario, S. M. & Laitinen, J. T. The serine hydrolases MAGL, ABHD6 and ABHD12 as guardians of 2-arachidonoylglycerol signalling through cannabinoid receptors. *Acta Physiologica* **204,** 267–276 (2012).
11. Ueda, N., Tsuboi, K. & Uyama, T. Metabolism of endocannabinoids and related N-acylethanolamines: Canonical and alternative pathways. *FEBS J.* **280,** 1874–1894 (2013).
12. Cravatt, B. F. *et al.* Molecular characterization of an enzyme that degrades neuromodulatory fatty-acid amides. *Nature* **384,** 83–87 (1996).
13. Mckinney, M. K. & Cravatt, B. F. Structure and function of Fatty Acid Amide Hydrolase. *Annu. Rev. Biochem.* **74,** 411–432 (2005).
14. O'Sullivan, S. E. in *Endocannabinoids* 393–422 (Springer, Cham, 2015). ISBN 9783319208251
15. Pacher, P., Steffens, S., Haskó, G., Schindler, T. H. & Kunos, G. *Cardiovascular effects of marijuana and synthetic cannabinoids: The good, the bad, and the ugly*. *Nature Reviews Cardiology* **15,** 151–166 (Nature Publishing Group, 2018).
16. Pacher, P. *et al.* Modulation of the endocannabinoid system in cardiovascular disease: therapeutic potential and limitations. *Hypertens. (Dallas, Tex. 1979)* **52,** 601–7 (2008).
17. Nomura, D. K. *et al.* Monoacylglycerol Lipase Regulates a Fatty Acid Network that Promotes Cancer Pathogenesis. *Cell* **140,** 49–61 (2010).
18. Chiang, K. P., Niessen, S., Saghatelian, A. & Cravatt, B. F. An Enzyme that Regulates Ether Lipid Signaling Pathways in Cancer Annotated by Multidimensional Profiling. *Chem. Biol.* **13,** 1041–1050 (2006).
19. Kimmel, C. B., Ballard, W. W., Kimmel, S. R., Ullmann, B. & Schilling, T. F. Stages of embryonic development of the zebrafish. *Dev. Dyn.* **203,** 253–310 (1995).
20. Link, B. A. & Megason, S. G. in *Source Book of Models for Biomedical Research* 103–112 (Humana Press, 2008). ISBN: 9781588299338
21. MacRae, C. A. & Peterson, R. T. Zebrafish as tools for drug discovery. *Nat. Rev. Drug Discov.* **14,** 721–731 (2015).
22. Rennekamp, A. J. & Peterson, R. T. 15 Years of Zebrafish Chemical Screening. *Curr. Opin. Chem. Biol.* **24,** 58–70 (2015).
23. Lieschke, G. J. & Currie, P. D. Animal models of human disease: Zebrafish swim into view. *Nature Reviews Genetics* **8,** 353–367 (2007).

24. Bowman, T. V. & Zon, L. I. Swimming into the future of drug discovery: In vivo chemical screens in zebrafish. *ACS Chem. Biol.* **5,** 159–161 (2010).
25. Zon, L. I. & Peterson, R. T. In vivo drug discovery in the zebrafish. *Nature Reviews Drug Discovery* **4,** 35–44 (2005).
26. Tay, T. L. *et al.* Proteomic analysis of protein profiles during early development of the zebrafish, Danio rerio. *Proteomics* **6,** 3176–3188 (2006).
27. Alli Shaik, A. *et al.* Functional mapping of the zebrafish early embryo proteome and transcriptome. *J. Proteome Res.* **13,** 5536–5550 (2014).
28. Kudoh, T. *et al.* A gene expression screen in zebrafish embryogenesis. *Genome Res.* **11,** 1979–1987 (2001).
29. White, R. J. *et al.* A high-resolution mRNA expression time course of embryonic development in zebrafish. *Elife* **6,** (2017).
30. Yu, P. B. *et al.* Dorsomorphin inhibits BMP signals required for embryogenesis and iron metabolism. *Nat. Chem. Biol.* **4,** 33–41 (2008).
31. Eddleston, M., Cohen, A. F. & Webb, D. J. Implications of the BIA-102474-101 study for review of first-into-human clinical trials. *British Journal of Clinical Pharmacology* **81,** 582–586 (2016).
32. Butler, D. & Callaway, E. Scientists in the dark after French clinical trial proves fatal. *Nature* **529,** 263–264 (2016).
33. Kerbrat, A. *et al.* Acute Neurologic Disorder from an Inhibitor of Fatty Acid Amide Hydrolase. *N. Engl. J. Med.* **375,** 1717–1725 (2016).
34. Bégaud, B. *et al.* BIA 10-2474: Minutes of the Temporary Specialist Scientific Committee (TSSC) meeting on 'FAAH (Fatty Acid Amide Hydrolase) Inhibitors'. *Meet. Minutes* 1–14 (2016).
35. Huggins, J. P., Smart, T. S., Langman, S., Taylor, L. & Young, T. An efficient randomised, placebo-controlled clinical trial with the irreversible fatty acid amide hydrolase-1 inhibitor PF-04457845, which modulates endocannabinoids but fails to induce effective analgesia in patients with pain due to osteoarthritis of th. *Pain* **153,** 1837–1846 (2012).
36. Li, G. L. *et al.* Assessment of the pharmacology and tolerability of PF-04457845, an irreversible inhibitor of fatty acid amide hydrolase-1, in healthy subjects. *Br. J. Clin. Pharmacol.* **73,** 706–716 (2012).
37. Hsu, K. L. *et al.* DAGLβ inhibition perturbs a lipid network involved in macrophage inflammatory responses. *Nat. Chem. Biol.* **8,** 999–1007 (2012).
38. Kolter, T. & Wendeler, M. Chemical chaperones - A new concept in drug research. *ChemBioChem* **4,** 260–264 (2003).
39. Jung, K.-M., Astarita, G., Thongkham, D. & Piomelli, D. Diacylglycerol lipase-alpha and -beta control neurite outgrowth in neuro-2a cells through distinct molecular mechanisms. *Mol. Pharmacol.* **80,** 60–7 (2011).
40. Thomas, G. *et al.* The Serine Hydrolase ABHD6 Is a Critical Regulator of the Metabolic Syndrome. *Cell Rep.* **5,** 508–520 (2013).
41. Pribasnig, M. A. *et al.* α/β hydrolase domain-containing 6 (ABHD6) degrades the late Endosomal/Lysosomal lipid Bis(Monoacylglycero)phosphate. *J. Biol. Chem.* **290,** 29869–29881 (2015).
42. Yoshino, H. *et al.* Postsynaptic diacylglycerol lipase α mediates retrograde endocannabinoid suppression of inhibition in mouse prefrontal cortex. *J. Physiol.* **589,** 4857–4884 (2011).
43. Lee, J. W. *et al.* Orphan GPR110 (ADGRF1) targeted by N-docosahexaenoylethanolamine in development of neurons and cognitive function. *Nat. Commun.* **7,** 13123 (2016).
44. Pool, M., Thiemann, J., Bar-Or, A. & Fournier, A. E. NeuriteTracer: A novel ImageJ plugin for automated quantification of neurite outgrowth. *J. Neurosci. Methods* **168,** 134–139 (2008).
45. Giepmans, B. N. G., Adams, S. R., Ellisman, M. H. & Tsien, R. Y. The fluorescent toolbox for assessing protein location and function. *Science* **312,** 217–224 (2006).

46. Phelps, M. E. Positron emission tomography provides molecular imaging of biological processes. *Proc. Natl. Acad. Sci.* **97,** 9226–9233 (2000).
47. van Rooden, E. J. *et al.* Mapping in vivo target interaction profiles of covalent inhibitors using chemical proteomics with label-free quantification. *Nat. Protoc.* **13,** 752–767 (2018).
48. Mann, M. & Jensen, O. N. Proteomic analysis of post-translational modifications. *Nature Biotechnology* **21,** 255–261 (2003).
49. Catherman, A. D., Skinner, O. S. & Kelleher, N. L. Top Down proteomics: Facts and perspectives. *Biochemical and Biophysical Research Communications* **445,** 683–693 (2014).
50. Khanna, I. Drug discovery in pharmaceutical industry: Productivity challenges and trends. *Drug Discovery Today* **17,** 1088–1102 (2012).
51. Bachovchin, D. A., Brown, S. J., Rosen, H. & Cravatt, B. F. Identification of selective inhibitors of uncharacterized enzymes by high-throughput screening with fluorescent activity-based probes. *Nat. Biotechnol.* **27,** 387–394 (2009).
52. Bachovchin, D. A. *et al.* A high-throughput, multiplexed assay for superfamily-wide profiling of enzyme activity. *Nat. Chem. Biol.* **10,** 656–663 (2014).
53. Geurink, P. P., Prely, L. M., Van Der Marel, G. A., Bischoff, R. & Overkleeft, H. S. Photoaffinity labeling in activity-based protein profiling. *Topics in Current Chemistry* **324,** 85–113 (2012).
54. Baggelaar, M. P. *et al.* Development of an activity-based probe and in silico design reveal highly selective inhibitors for diacylglycerol lipase-α in brain. *Angew. Chemie - Int. Ed.* **52,** 12081–12085 (2013).
55. Van Esbroeck, A. C. M. *et al.* Activity-based protein profiling reveals off-target proteins of the FAAH inhibitor BIA 10-2474. *Science* **356,** 1084–1087 (2017).
56. Labun, K., Montague, T. G., Gagnon, J. A., Thyme, S. B. & Valen, E. CHOPCHOP v2: a web tool for the next generation of CRISPR genome engineering. *Nucleic Acids Res.* **44,** W272–W276 (2016).
57. Ran, F. A. *et al.* Genome engineering using the CRISPR-Cas9 system. *Nat Protoc* **8,** 2281–2308 (2013).
58. Cong, L. *et al.* Multiplex genome engineering using CRISPR/Cas systems. *Science* **339,** 819–823 (2013).